Chapter 7

Design of an Energy Management System for Secure Integration of Renewable Energy Sources into Microgrids

Luis I. Minchala, Youmin Zhang and Oliver Probst

Additional information is available at the end of the chapter

http://dx.doi.org/10.5772/intechopen.69399

Abstract

This chapter presents the design and development of an energy management system (EMS), which guarantees a secure operation of an islanded microgrid under possible imbalances between generation capacity and loads demand. The EMS performs an optimal calculation of low priority loads to be shed, as well as charging and discharging cycles of batteries within the microgrid. A nonlinear model-predictive control (NMPC) algorithm is selected for implementing the EMS, which processes a data set composed of loads measurements, generation capacity, batteries state of charge (SOC), and a set of operation constraints. The EMS is designed under the assumption of having an advanced metering infrastructure (AMI) installed in the microgrid. The EMS is tested in a simulation platform that integrates models of the microgrid components, as well as their distributed controllers (DCs). Simulation results show the effectiveness of the proposed approach, since critical variables as the microgrid's frequency and voltage magnitude operate within a secured interval even under the presence of faults in one of the DCs.

Keywords: energy management, microgrid, fault-tolerant control, smart grids, power flow

1. Introduction

Many inventions have evolved over time from their initial conception, for example, the telephone. The telephone invention triggered a revolution in communications around the world that led to the powerful technology we have today. Alexander Graham Bell would be proud of his invention because of the impact and evolution of telephone, from landlines to satellite

communications, the Internet, and so on. Another important invention is electricity. According to Ref. [1], electricity is the most important engineering invention of the last century. Electric networks' evolution led to a power system composed of three main systems: *generation*, *transmission*, and *distribution*. The main objective of the electric power system is to guarantee an efficient delivery of energy to end users. In the last 10 years, there has been a continuous search for emerging technologies, which foster green-energy integration into the main grid. In addition, stakeholders of the power grid have also changed their functionality in the system. Today, consumers are no longer just consumers, they can also be generators and their consumption and generation must be carefully regulated. This is the world of the smart grids (SGs) [2], where it is possible to have small isolated power systems operating as standalone islands purposefully. These islands are called *microgrids*.

A key objective of SGs is to provide reliable power supply through a combination of monitoring, control, and response. Electric utilities are expected to provide continuous and high-quality services to their customers at reasonable prices by making economical use of available infrastructure. The most powerful force shaping the future of power industry is economics, but environmental protection is receiving growing attention today. Global warming trend could be damped through energy conservation. Therefore, any new innovations/trends will probably be adopted only if they reduce costs and CO_2 emissions.

The development of an intelligent power distribution system requires new approaches. Reference [3] provides a French vision of SGs, which shows that distributed generation (DG) has strongly increased in the last 10 years. By 2020, the European Union targets 20% of the energy consumed to be generated by renewable energy sources (RESs). A technical report on the development of an intelligent distribution automation system in Korea [4] describes the following system features: remote operation, management of low voltage (LV) and medium voltage (MV) networks supported on a geographic information system (GIS), loss minimization, volt/var control for integrated DG, and power quality monitoring. Reference [5] details the features of an automatic power restoration system, which integrates DCs, distributed intelligence, and peer-to-peer communication to isolate faults and restore power to unfaulted sections. Further information about active microgrids projects around the world, including details on technical operational aspects and design criteria, can be found in the survey papers [6, 7].

2. Smart grids overview

The SG is defined as an electrical network that integrates in a smart way every action of the users plugged into it—generators, consumers, and those that can perform both actions, delivering electricity efficiently, sustainably, economically, and safely.

2.1. Distributed generation

A DG unit is a small-scale generation source with its output ranging from 1 KW to several MW and usually installed at the distribution level. A particular characteristic of DG is that the generating sources are near end users. As RESs penetrate the utility systems, the power industry

http://dx.doi.org/10.5772/intechopen.69399

undergoes a paradigm shift that will change the industry to the use of DG systems. **Figure 1** illustrates the DG concept by showing three different locations with installed DG units.

Small generators, which transform energy from RES, can be incorporated in the electric distribution network, for example, wind turbine generator (WTG) and photovoltaic (PV) arrays. These energy sources present many challenges to researchers and designers regarding power quality and economic issues. Today's power systems rely on spinning reserve and drooping frequency-load characteristics. Future systems, on the other hand, will rely on RES, which operate at peak power in order to displace as much fuel consumption as possible. This peak power constraint imposed by wind and sun complicates the frequency/load control of the entire system [8]. In order to compensate for this intermittent and changing power, short- and long-term storage devices should be deployed. Storage devices can be charged during periods of low-power demand and can supply power during high-power demand. This concept is shown in **Figure 2**.

2.2. Microgrids

Microgrids are small-scale LV/MV power systems with distributed energy resources (DERs), storage devices, and controllable loads, connected to the main power network or islanded, in

Figure 1. DG overview.

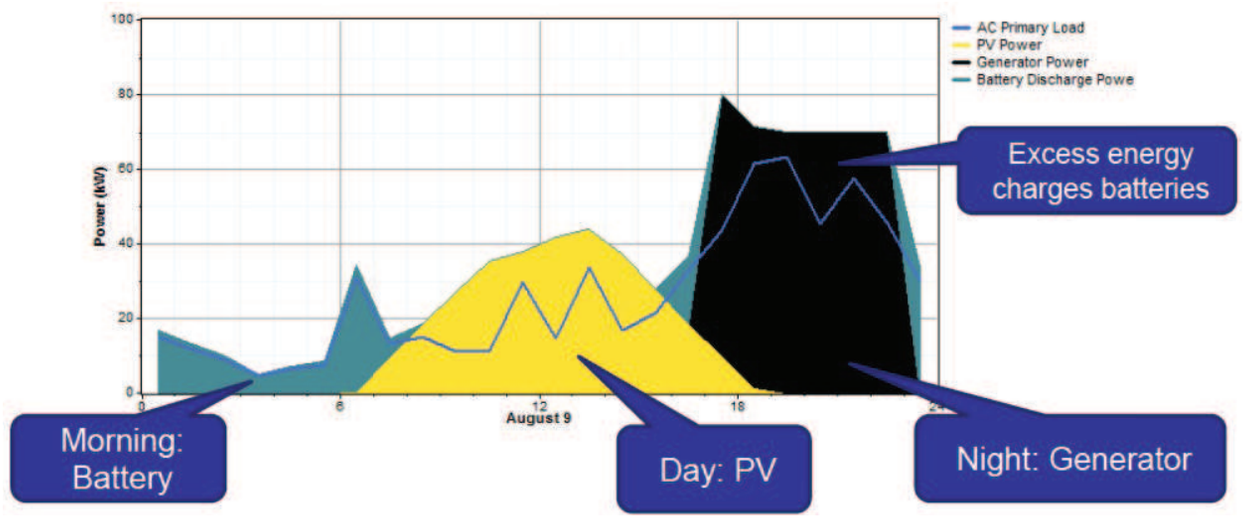

Figure 2. Example of an energy dispatch strategy for a microgrid.

a controlled and coordinated way [9]. Microgrids have different operating characteristics than bulk power systems (BPSs). A comparison, between microgrids and BPS, is shown in **Table 1**. Microgeneration units, typically located at users' sites, have emerged as a promising option to meet growing customer needs for electric power with an emphasis on reliability, power quality, and contribution to different economic, environmental, and technical benefits. However, the impact of microgeneration at LV levels on power balance and grid frequency is still a great challenge.

2.3. Advanced metering infrastructure

Smart meters (SMs) are important components of SGs. These devices have the following main features: full-duplex communication, ability to connect or disconnect consumer's loads, and recording capabilities for capturing waveforms for supervising voltage and current. SMs are gradually replacing traditional meters currently in operation and are also being installed in new microgrids. SMs transmit information to different information clients via SCADA systems and other networks.

Among the benefits that SMs offer to consumers, there is the possibility to know in real-time rates and pricing policies, allowing users to decide wisely how to use electric energy. Several research papers are devoted to household scheduling using AMI in order to reduce power consumption during peak consumption hours [10, 11]. **Figure 3** shows a possible architecture for an AMI. Due to the large number of SMs that will be available in distribution systems, the potential ability of SMs to provide additional information for outage management is also being investigated [12].

2.4. Fault-tolerant control

Critical-safety and operability issues with a defined performance in technological systems, such as electrical, industrial, aircraft control, nuclear generation, and so on, cause them to rely on complex control systems. Classic control schemes are suitable for guaranteeing a desired system performance in a specific operating range. However, these control strategies are unable to maintain the system performance under faulty scenarios. Therefore, there is a necessity of fault-tolerant control (FTC) strategies to improve the reliability and availability of critical-safe systems.

Quick detection of faults avoids serious damages to machines and humans, while allowing online reconfiguration of fault-tolerant controllers. Many books and research papers related to the field of FTC coincide on a two-step methodology for making a system fault-tolerant [13, 14]:

	RES penetration	Energy storage	Voltage levels	Dispatch objects	Operation mode
Microgrid	High	Yes	LV and MV	Controllable generators and loads	Grid-connected and autonomous
BPS	Low	Negligible	HV	Controllable generators	Independent operation

Table 1. Comparison between microgrids and BPS.

http://dx.doi.org/10.5772/intechopen.69399

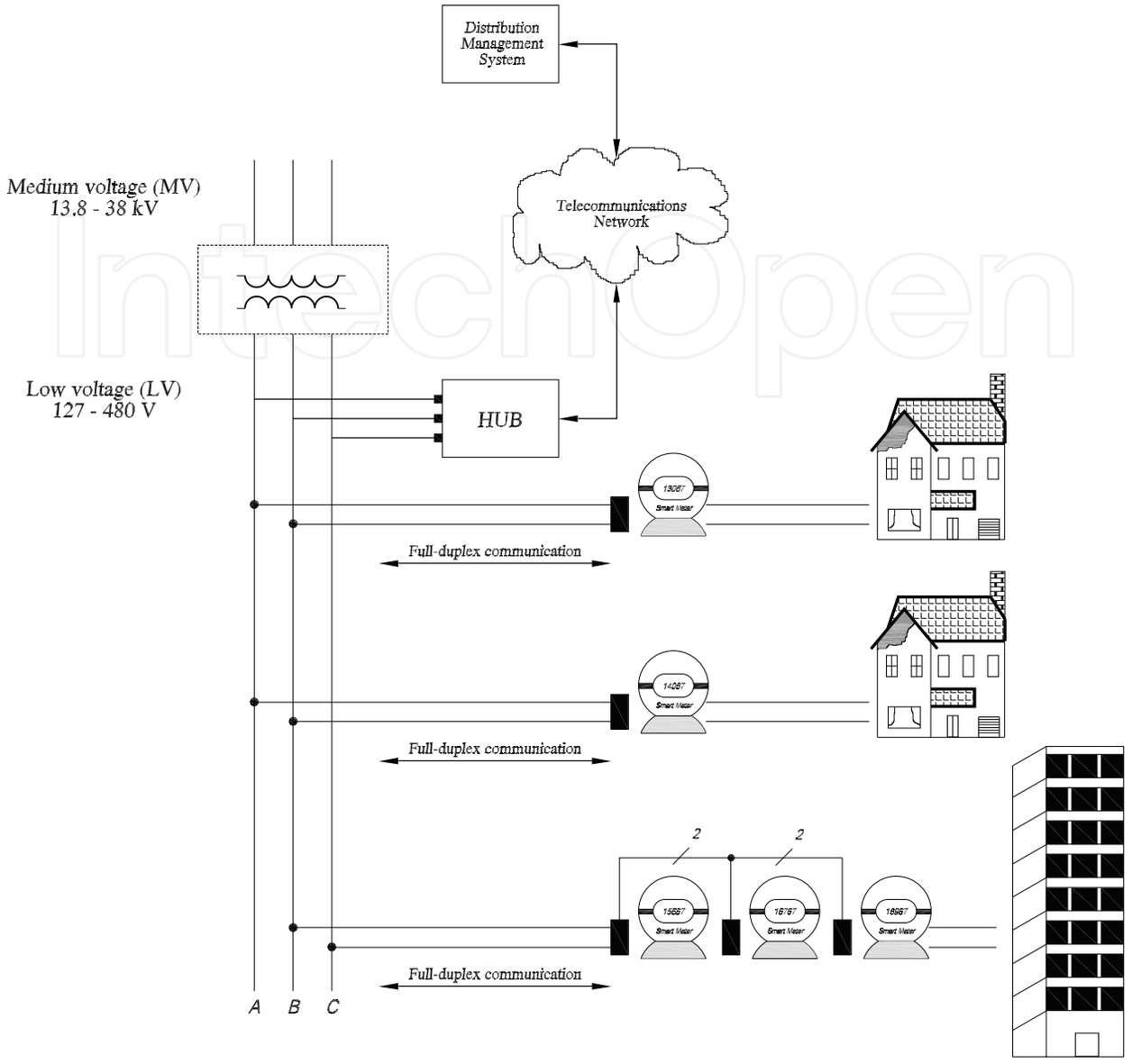

Figure 3. Remote management system for electricity measurement.

1. Fault diagnosis: Whenever a fault is present in the system, it has to be detected and identified.
2. Control reconfiguration: The controller has to be designed with the ability to accommodate faults on components automatically.

This methodology is an active research field, mainly due to the variety of possibilities for executing the abovementioned steps. Fault diagnosis is performed by a fault detection and diagnosis (FDD) module, while control reconfiguration could be done by many different control approaches, such as model-based, intelligent, gain scheduling, and so on. Such an FTC system, which relies on the fault information obtained from the FDD module, is called an active fault-tolerant control system (AFTCS). **Figure 4** shows an architecture of an AFTCS [14].

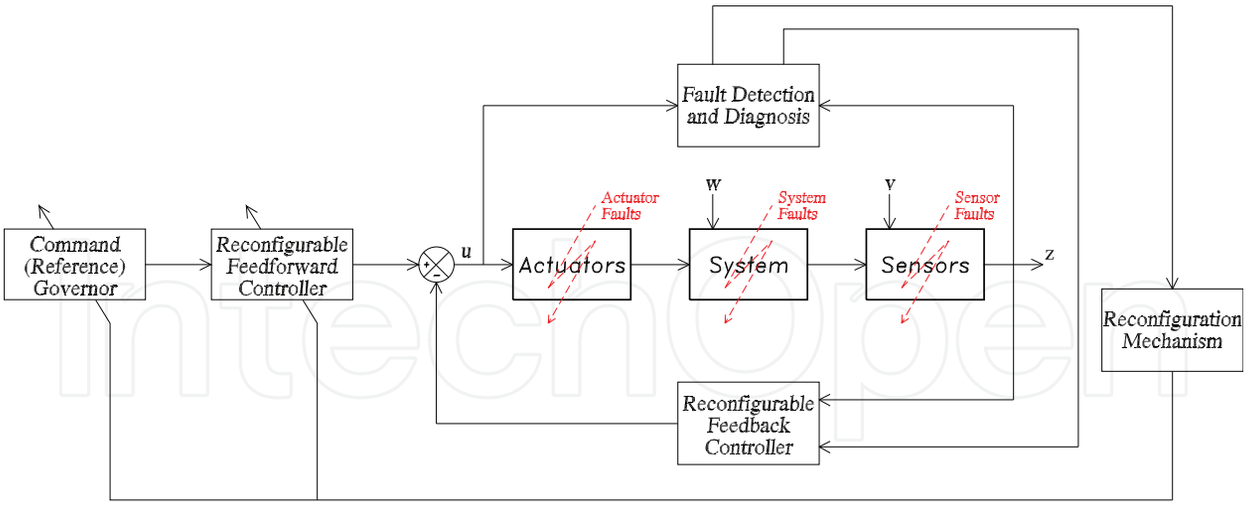

Figure 4. A general structure of an AFTCS [14].

3. Microgrid modeling

Control engineering most of the times is model dependent. Understanding the process, system, or plant to be controlled is fundamental for proposing proper control strategies. This section presents modeling procedures of the microgrid components used throughout this research: diesel engine generator (DEG), WTG, PV array, battery storage system (BSS), and power converters. At the end of this section, a microgrid benchmark model is presented, which integrates the microgrid components in one single simulation environment. **Figure 5** shows the aforementioned elements in a microgrid configuration.

The rationale for the SGs lies in the integrative analysis of DERs, many of which will be intermittently operating, with the deployment of short-term and long-term storage systems. Current strategies on load sharing will not work to integrate RES due to its peak-power and intermittent operation. Therefore, new control strategies for voltage/reactive-power and load-sharing/frequency need to be developed; microgrid modeling is the first step prior to advanced controllers design.

3.1. DG units modeling

A DG unit is conformed mainly of three components:

1. Microgeneration unit. Typical choices are batteries, PV, WTG, flywheels, fuel cells, and so on.
2. Power conditioning system (PCS). PCS is related with power conversion, AC/DC or DC/AC, and its control techniques.
3. Coupling circuit. Interface elements, most of the times a filter, for coupling the DG unit with the network.

http://dx.doi.org/10.5772/intechopen.69399

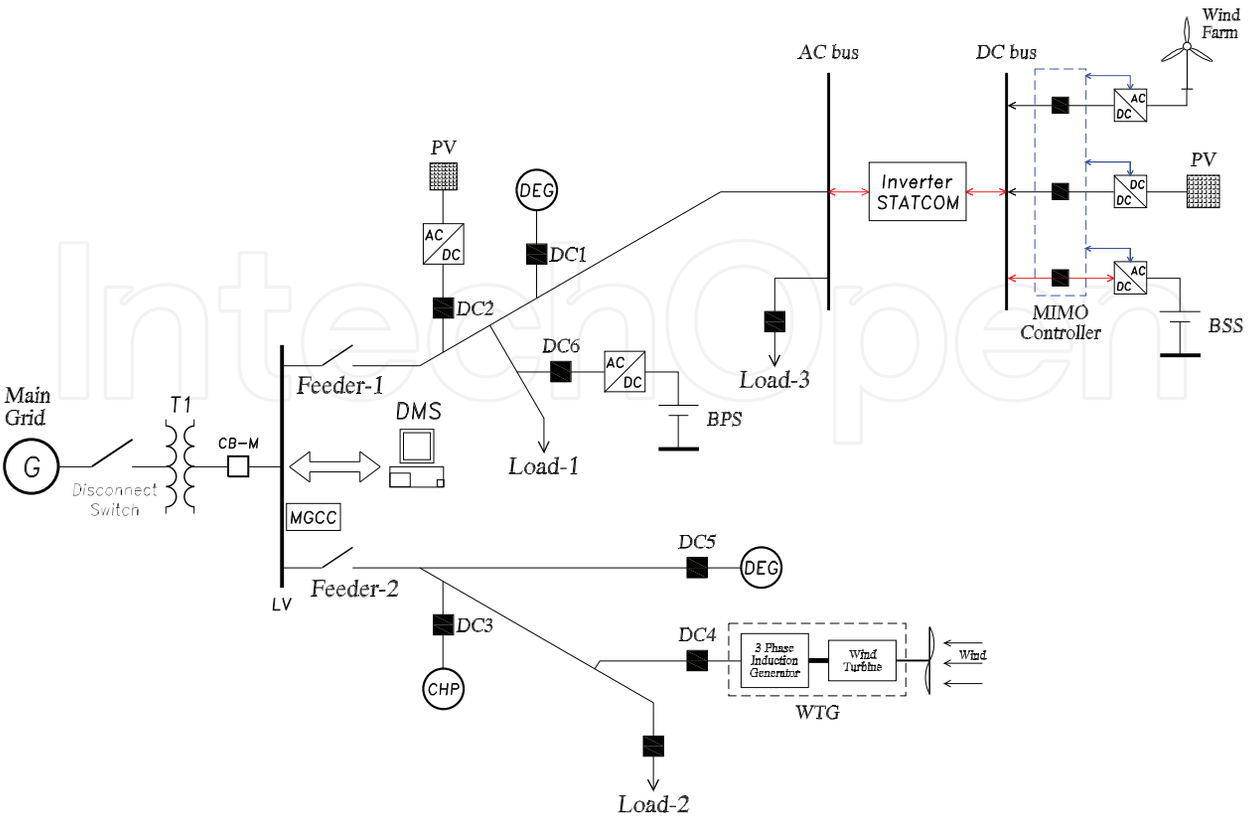

Figure 5. Microgrid control and management system architecture.

3.1.1. Power electronic converters

Proper integration technology has to be developed for using DG units in a microgrid configuration. The majority of DG units is integrated to the grid through the use of power electronics-based interfaces, which convert the power, firstly, to DC and then puts the energy into the grid by using an inverter. Adequate control strategies of the PCS allow maximum extraction of the energy from RES.

Power electronic converters performing conditioning have to be highly efficient, flexible, and reliable. It is well known that improving the performance of power converters increases system's efficiency. According to **Figure 5**, there are mainly three power electronic circuits that need to be implemented to control voltage, power, and frequency of a DG unit: AC/DC converter, DC/DC converter, and voltage source inverter (VSI).

3.1.2. Diesel engine generator

Diesel generating sets are typically used in power systems without connection to the power grid, as emergency power supply if the grid fails, as well as for more complex applications such as peak-shaving, grid support, and energy export to the power grid. This section presents models for the diesel engine (DE) components: synchronous generator and diesel engine.

3.1.2.1. Synchronous machine model

The synchronous generator has two circuits magnetically coupled: the first one is static and has the shape of a hollow cylinder with longitudinal slots and an armature winding; the second component is the rotor whose winding is supplied with DC current. The DC current is supplied to the field winding by an exciter, which may be a generator mounted on the same shaft or a separate DC source connected to the field winding through brushes bearing on slip rings [15].

As a prime mover drives the machine shaft, the magnetic field generated by the field winding links the stator coils to induce voltage in the armature windings.

As presented in Ref. [16], a state-space model, which uses the *dq* dynamic equations of the electrical circuit of a synchronous generator with a pure resistive load (RL) connected to its terminals, can be represented as follows:

$$\mathbf{L}\frac{d\mathbf{x}}{dt} = \mathbf{A}\mathbf{x} + \mathbf{B}v_F$$

$$\mathbf{x} = [i_d \quad i_q \quad i_F]^T$$

$$\mathbf{A} = \begin{bmatrix} -(R_s + R_L) & \omega L_s & 0 \\ -\omega L_s & -(R_s + R_L) & -\omega L_m \\ 0 & 0 & -R_F \end{bmatrix} \qquad \mathbf{L} = \begin{bmatrix} L_s & 0 & L_m \\ 0 & L_s & 0 \\ L_m & 0 & L_F \end{bmatrix} \qquad \mathbf{B} = \begin{bmatrix} 0 \\ 0 \\ 1 \end{bmatrix} \tag{1}$$

where $[i_d \ \ i_q \ i_F]^T$ are the *dq* stator and field currents, respectively; R_s and R_F are the stator and field resistances; L_s, L_m, and L_F are the stator, magnetizing, and field inductances; ω is the electrical speed; v_d and v_q are the *dq* stator voltages; and v_F is the field voltage which will be used as a control input.

3.1.2.2. Diesel engine model

The DE contains the combustion system and is responsible for the movement of the pistons, consequently the movement of the crankshaft that generates the output torque T(s). **Figure 6** shows a block diagram of a DE. A first-order system models the actuator dynamics of the DE. The time delay $e^{-\tau s}$ and a torque constant K_b model the combustion system. The flywheel block

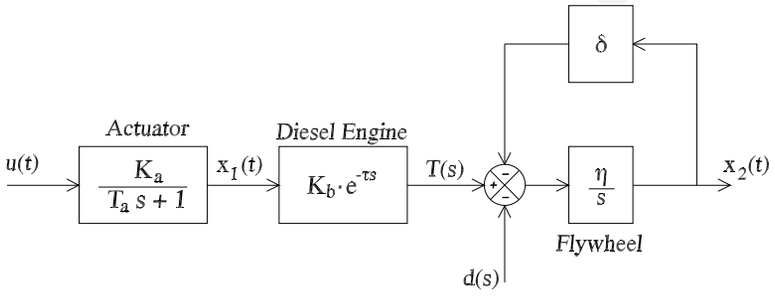

Figure 6. DE block diagram [6].

System parameter	Value range	Nominal range
Actuator gain constant K_a (pu)	1.0	1.0
Actuator time constant T_a (s)	0.05–0.2	0.125
Engine torque constant K_b (pu)	0.8–1.5	1.15
Engine dead time t (s)	0–1	0.5
Plant and flywheel acceleration δ (s^{-1})	0.1–0.5	0.3
Friction coefficient η (pu)	0.1	0.1

Table 2. System parameters of a typical DE.

models the inertia generated inside the machine, η represents the flywheel acceleration constant, and the coefficient δ represents friction. The fuel injected to the DE is represented by $x_1(t)$, whereas $x_2(t)$ represents the angular velocity of the engine's shaft. d(s) models load changes in the rotor's shaft.

$$\dot{x}_1(t) = -\frac{1}{T_a}x_1(t) + \frac{K_a}{T_a}u(t)$$
$$\dot{x}_2(t) = \eta K_b x_1(t\text{-}\tau) - \eta x_2(t) \tag{2}$$

Table 2 shows the characteristic values of the DE constants of model (2).

3.1.3. Wind-driven generation system

This section presents details on the modeling of a wind-driven electricity generation system (WEGS). A horizontal axis wind turbine (WT) is chosen as prime mover, while an induction generator performs the energy conversion. The wind turbine induction generator is an attractive DG unit in a deregulated electric energy market since wind energy is a non-polluting source.

Wind energy is air in motion whose energy is derived from sun, because about 2% of the solar flux falling on earth's surface is transformed into wind due to uneven heating of the atmosphere. Wind energy has some limiting characteristics such as non-schedulability, uncontrollable, and so on.

3.1.3.1. Wind turbine model

The WT model used throughout this chapter is a lumped mass model. The WT is pitch controlled through the blade pitch angle, β. The power coefficient, C_p as shown in Eq. (3), characterizes the WT and depends on the tip speed ratio, $\lambda = \Omega R/V_w$, and β, where R is the WT rotor radius, Ω is the mechanical angular velocity of the WT rotor, and V_w is the wind velocity. The pitch angle β is only varied to limit the over-speed of the generator

$$C_p(\lambda,\beta) = 0.5716(116\kappa\text{-}0.4\beta - 5)e^{-21\kappa} + 0.0068\lambda$$
$$\kappa = \left(\frac{1}{\lambda + 0.08\beta} - \frac{0.035}{\beta^3 + 1}\right) \tag{3}$$

The dynamic output mechanical torque of the WT, $T_{m,}$ is expressed as

$$T_m = \frac{\rho A R C_p V_w^3}{2\lambda} \tag{4}$$

where ρ is the air density and A represents the swept area of the blades.

3.1.3.2. Induction generator model

The electrical equations of the induction generator model in the *dq* reference frame can be expressed in pu as

$$\begin{aligned}
v_{qs} &= r_s i_{qs} + \frac{\omega}{\omega_b}\psi_{ds} + \frac{p}{\omega_b}\psi_{qs} \\
v_{ds} &= r_s i_{ds}\text{-}\frac{\omega}{\omega_b}\psi_{qs} + \frac{p}{\omega_b}\psi_{ds} \\
v'_{qr} &= r'_r i'_{qr} + \left(\frac{\omega\text{-}\omega_r}{\omega_b}\right)\psi'_{dr} + \frac{p}{\omega_b}\psi'_{qr} \\
v'_{dr} &= r'_r i'_{dr} + \left(\frac{\omega\text{-}\omega_r}{\omega_b}\right)\psi'_{qr} + \frac{p}{\omega_b}\psi'_{dr} \\
\frac{p}{\omega_b}\omega_r &= \frac{1}{2H}(T_e\text{-}T_0) \\
T_e &= \psi'_{qr} i'_{dr}\text{-}\psi'_{dr} i'_{qr}
\end{aligned} \tag{5}$$

where $v_{s,}$ $v_{r,}$ $i_{s,}$ $i_{r,}$ $\Psi_{s,}$ and Ψ_r represent the voltage, current, and flux (subscript s stands for stator and subscript r for rotor); r_s and r_r are stator and rotor resistance, respectively; ω_r is the rotor angular speed; ω_b is the base electrical angular velocity; H represents inertia moment, T_0 is load torque, and p denotes a time derivative operation.

3.1.4. Photovoltaic generation system

A PV cell is represented as a single-diode mathematic model, which is composed of a current source $I_{ph,}$ a nonlinear diode, and internal resistances, R_s and R_{sh}. **Figure 7** shows the PV cell model.

A PV array is composed of the combination of N_p parallel and N_s serial PV cells. The total current produced by a PV array is expressed as follows:

$$i(t) = N_p i_{ph} - N_p I_s \left(e^{\frac{q}{AkT}\left(\frac{V}{N_s}+\frac{iR_s}{N_p}\right)} - 1 \right) - \frac{N_p}{R_{sh}} \left(\frac{V}{N_s} + \frac{iR_s}{N_p} \right) \tag{6}$$

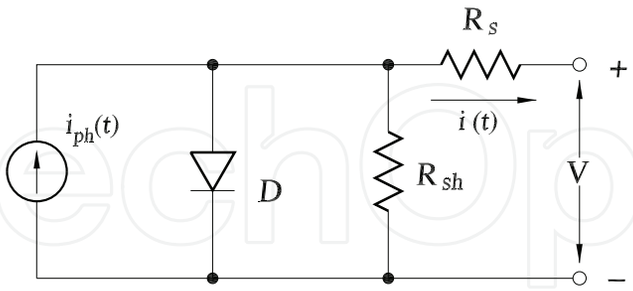

Figure 7. Single diode PV model.

3.1.5. Battery model

An electrical battery is one or more electrochemical cells that convert stored chemical energy into electrical energy. The lead-acid battery is the oldest type of rechargeable battery with a low energy-to-weight ratio. Lead-acid batteries are fully charged if it is possible to measure an open-circuit voltage of fully discharged battery cell(s). The term discharged means that all free charges are zero and the only voltage source is the cell(s) voltage, V_0 [17].

References [18, 19] present a simple nonlinear Thevenin model for the lead-acid battery. This model considers the dynamic response of the battery, which is influenced by the capacitive effects of the battery plates and also by the charge-transfer resistance. **Figure 8** shows the equivalent circuit of a lead-acid battery

$$V_0 = R_d C \frac{dV_p(t)}{dt} + \frac{1}{C} i_B(t) + \frac{1}{R_d C} V_0$$

$$\frac{dV_p(t)}{dt} = -\frac{1}{R_d C} V_p(t) - \frac{1}{C} i_B(t) + \frac{1}{R_d C} V_0 \tag{7}$$

$$V_B(t) = V_p(t) - R_B i_B(t)$$

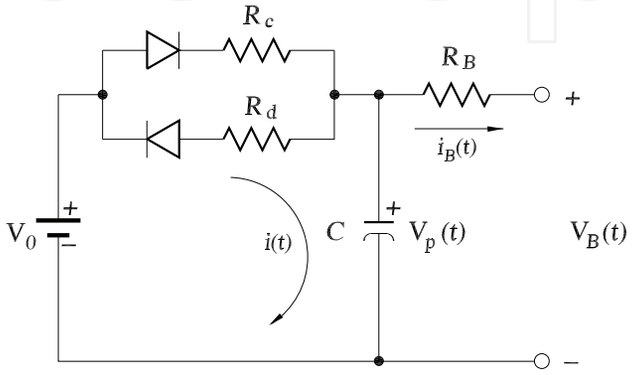

Figure 8. Nonlinear lead-acid battery equivalent circuit.

3.2. Microgrid model

Operating a microgrid within the limits of the established operation standards requires the development of novel control strategies. According to the standard ANSI C84.1, utilities are required to maintain voltage at the customer's service panel between 114 and 126 V (±5%)

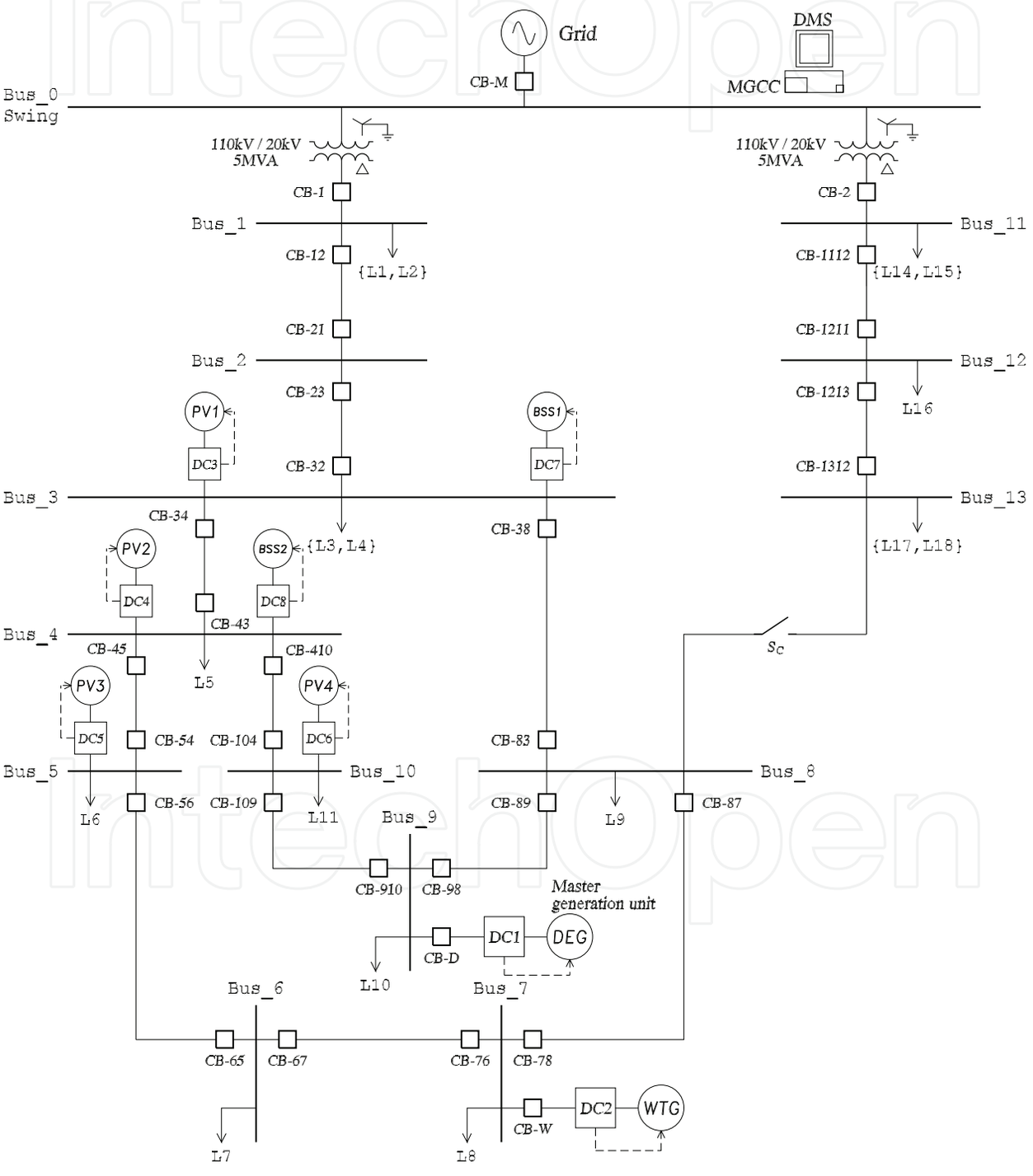

Figure 9. Microgrid MV benchmark model CIGRE TF C6.04.02.

based on a 120-V nominal secondary voltage. Standard IEEE 1547-2-2011 [20] recommends that for interconnecting DERs with electric power systems, the total time should be less than 0.15 s when the magnitude of the frequency variation exceeds 0.5 Hz and the magnitude of the voltage variation exceeds 5%.

Figure 9 shows the microgrid benchmark model configuration, consisting of two feeders supplied by a distribution substation. A grid of DG units is connected to the left-side feeder, including four PV array units, one WTG, two BSS, and one DEG. Every DG unit has a DC. The rated voltage level of the network is 20 KV, which is supplied from a 110 KV transformer station. The parameters of the network, the load and the DG units (in pu), were taken from Ref. [21] and are summarized in **Tables 3** and **4**.

Although maximum values for active and reactive power loads are considered in the network parameters shown in **Table 3**, variable load profiles have been generated for loads L_1, L_2, L_6, L_7, and L_9.

The features of DG units are as follows

- DEG: As previously described, a DE is used as the prime mover of a synchronous generator. The system frequency is determined by the DE mechanical speed ω_m, and the synchronous

Load no.	Load type	P_{max} (*pu*)	Q_{max} (*pu*)
1	Residential	0.15000	0.03100
2	Industrial	0.05000	0.01000
3	Residential	0.00276	0.00069
4	Industrial	0.00224	0.00139
5	Residential	0.00432	0.00108
6	Residential	0.00725	0.00182
7	Residential	0.00550	0.00138
8	Industrial	0.00077	0.00048
9	Residential	0.00588	0.00147
10	Industrial	0.00574	0.00356
11	Industrial	0.00068	0.00042
12	Residential	0.00477	0.00120
13	Residential	0.00331	0.00083
14	Residential	0.15000	0.03000
15	Industrial	0.05000	0.01700
16	Industrial	0.00032	0.00020
17	Industrial	0.00330	0.00020
18	Residential	0.00207	0.00052

Table 3. Load parameters of the microgrid model.

From	To	*R*	*X*	*C*	*L*
Node	**Node**	**(Ω/km)**	**(Ω/km)**	**(nF/km)**	**(km)**
0	1				
1	2	0.579	0.367	158.88	2.82
2	3	0.164	0.113	6608	4.42
3	4	0.262	0.121	6480	0.61
4	5	0.354	0.129	4560	0.56
5	6	0.336	0.126	5488	1.54
6	7	0.256	0.130	3760	0.24
7	8	0.294	0.123	5600	1.67
8	9	0.339	0.130	4368	0.32
9	10	0.399	0.133	4832	0.77
10	11	0.367	0.133	4560	0.33
11	4	0.423	0.134	4960	0.49
3	8	0.172	0.115	6576	1.3
0	12				
12	13	0.337	0.358	162.88	4.89
13	14	0.202	0.122	4784	2.99

Table 4. Transmission line parameters.

generator field current sets the voltage magnitude. The rated output power of the DEG is 0.3125 pu over a P_{base} of 5 MW.

- WTG: The characteristics of WTG are assumed in Section 3.1.3. The maximum output power of the WTG is 0.2 pu.
- PV array: The features of the PV modules 330 SunPower (SPR-305) are used. PV_1 array consists of 66 strings of five series-connected modules connected in parallel, providing 0.02 pu. PV_2, PV_3, and PV_4 have 0.02, 4×10^{-3}, and 5×10^{-3} pu of power generation capacity, respectively. The PCS of every PV array is composed of a boost converter and a VSC.
- BSS: The lead-acid batteries are combined with bidirectional DC/AC converters with a maximum output power of 0.02 pu for BSS1 and 0.015 pu for BSS2. The charging power for every BSS is 0.01 pu.

DERs do not provide system frequency regulation. Therefore, for power flow calculations, the DG units (except for the DEG) are considered as load nodes with negative power consumption. During grid-connected operation, the main grid controls voltage and frequency. Islanded operation demands that local microgrid generation controls voltage and frequency.

4. Energy management system

The system states for the islanded section (left-side feeder) of the distribution system in **Figure 9** are defined as

$$\mathbf{x} = \begin{bmatrix} \mathbf{x_1} \\ \mathbf{x_2} \end{bmatrix} \qquad \begin{matrix} \mathbf{x_1} \in \mathbb{R}^{10} & \mathbf{x_1} = [V_i]^T & i = 1, 2, \ldots, 10 \\ \mathbf{x_2} \in \mathbb{R}^{10} & \mathbf{x_2} = [\delta_i]^T & i = 1, 2, \ldots, 10 \end{matrix} \tag{8}$$

where V_i and δ_i are node's voltage and angle of the bus i.

Additionally, more variables and vectors are needed for the controller formulation, such as power at the nodes $S_i = P_i + jQ_i$, admittance matrix Y, and power generated by the DG units, P_{DGi}:

$$Y = [Y_{i,j}]$$
$$S = \begin{bmatrix} \mathbf{P_{load}} \\ \mathbf{Q_{load}} \end{bmatrix} \qquad \begin{matrix} \mathbf{P_{load}} \in \mathbb{R}^{10} & \mathbf{P_{load}} = [P_{Li}]^T & i = 1, 2, \ldots, 10 \\ \mathbf{Q_{load}} \in \mathbb{R}^{10} & \mathbf{Q_{load}} = [Q_{Li}]^T & i = 1, 2, \ldots, 10 \end{matrix} \tag{9}$$

$$\mathbf{P}_{DG} = \left[P_{DG_i}\right]^T \qquad i = 1, 2, \ldots, 8 \begin{cases} i = 1, \text{ Diesel engine power } (P_{DE}) \\ i = 2, \text{ Wind turbine power } (P_{WT}) \\ i = 3, PV\ power\ array\ 1\ \left(P_{PV_1}\right) \\ i = 4, PV\ power\ array\ 2\ \left(P_{PV_2}\right) \\ i = 5, PV\ power\ array\ 3\ (P_{P3}) \\ i = 6, PV\ power\ array\ 4\ \left(P_{PV_4}\right) \\ i = 7, Power\ in\ BBSS\ 1\ \left(P_{BSS_1}\right) \\ i = 8, Power\ in\ BBSS\ 2\ \left(P_{BSS_2}\right) \end{cases} \tag{10}$$

$$S_i = V_i \sum_{m=1}^{N} (Y_{im} Vi)^* \tag{11}$$

Equation (11) is solved iteratively through the Newton-Raphson (NR) power flow algorithm, with prior knowledge of P_{DGi}, and current load consumption of every power system node. P_{DE} is estimated in a prediction horizon of length N. An important modification of Eq. (11) is the inclusion of the reactive power consumed by the WTG at bus 7, which is calculated as follows [22]:

$$Q_{WT} = -\frac{V_7^2}{z_p} + \frac{-V_7^2 + \sqrt{V_7^4 - 4P_7 z^2}}{2z}$$
$$z = z1 + z2 \qquad z_p = \frac{z_c z_m}{z_c - z_m} \tag{12}$$

where the negative sign of Eq. (12) represents reactive power consumption of the WTG induction generator from the network; z_m, z_c, z_1, and z_2 represent the excitation reactance, reactance of a capacitor bank installed at the terminal of the induction generator, and the stator and rotor reactance, respectively.

The control objectives of the proposed strategy are as follows:

- To manage the connection and disconnection events of batteries;
- To shed low priority loads every time the load demand is greater than the generation capacity. This control action anticipates any harmful operation of the system through the predicting model, which predicts potential load imbalances;
- To keep the voltage magnitude with a maximum variation of ±5%.

A microgrid-centralized controller (MGCC) implements an NMPC algorithm. Loads management as well as batteries connecting and disconnecting events are performed by a control vector, **u**, defined by Eq. (13). The control vector is calculated in real time by the MGCC, and transmitted to the DCs in the microgrid. **Table 5** presents the relationship between each bit of **u** and its corresponding load controller for switching purposes, that is, for $u_i = 1 \rightarrow L_i$ load is connected, and for $u_i = 0 \rightarrow L_i$ load is disconnected

$$\mathbf{u} = [u_i] \qquad i = 1, 2, \ldots, 13 \qquad u_i \text{ is a binary signal} \tag{13}$$

An important requirement in the design of NMPC is the availability of a model for predicting the output variables. The NMPC algorithm requires predicted values of the power generated by the DEG to optimally decide which load has to be shed. Trip commands are sent from the MGCC to proper loads. **Figure 10** shows the EMS architecture. This control architecture is deeply analyzed in Ref. [23].

Control signal	Load	Observations
$u1$	L1* = {L1 U L2}	Variable loads
$u2$	L3 U L4	Constant loads
$u3$	L5	Constant load
$u4$	L6	Variable load
$u5$	L7	Variable load
$u6$	L8	Constant load
$u7$	L9	Constant load
$u8$	L10	Constant load
$u9$	L11	Constant load
$u10$	BSS1	Charge mode
$u11$	BSS1	Discharge mode
$u12$	BSS2	Charge mode
$u13$	BSS2	Discharge mode

Table 5. Control vector correspondence with loads and BSS.

http://dx.doi.org/10.5772/intechopen.69399

The NR power flow algorithm is used to predict the microgrid's system states, and consequently the P_{DE} in a specific prediction horizon N. To find the optimal steady-state operation of the microgrid, the connection and disconnection commands of the control vector **u** are accounted within the NR algorithm. An initial data set Z_k composed of the batteries' SOC, load demand, and the active power generated by every DER is required prior to the execution of the NR calculation. The data set Z_k does not consider load variations within the prediction horizon. This fact is considered, and two approaches were tested for the initial iterative load values of the NR algorithm in order to predict P_{DE}:

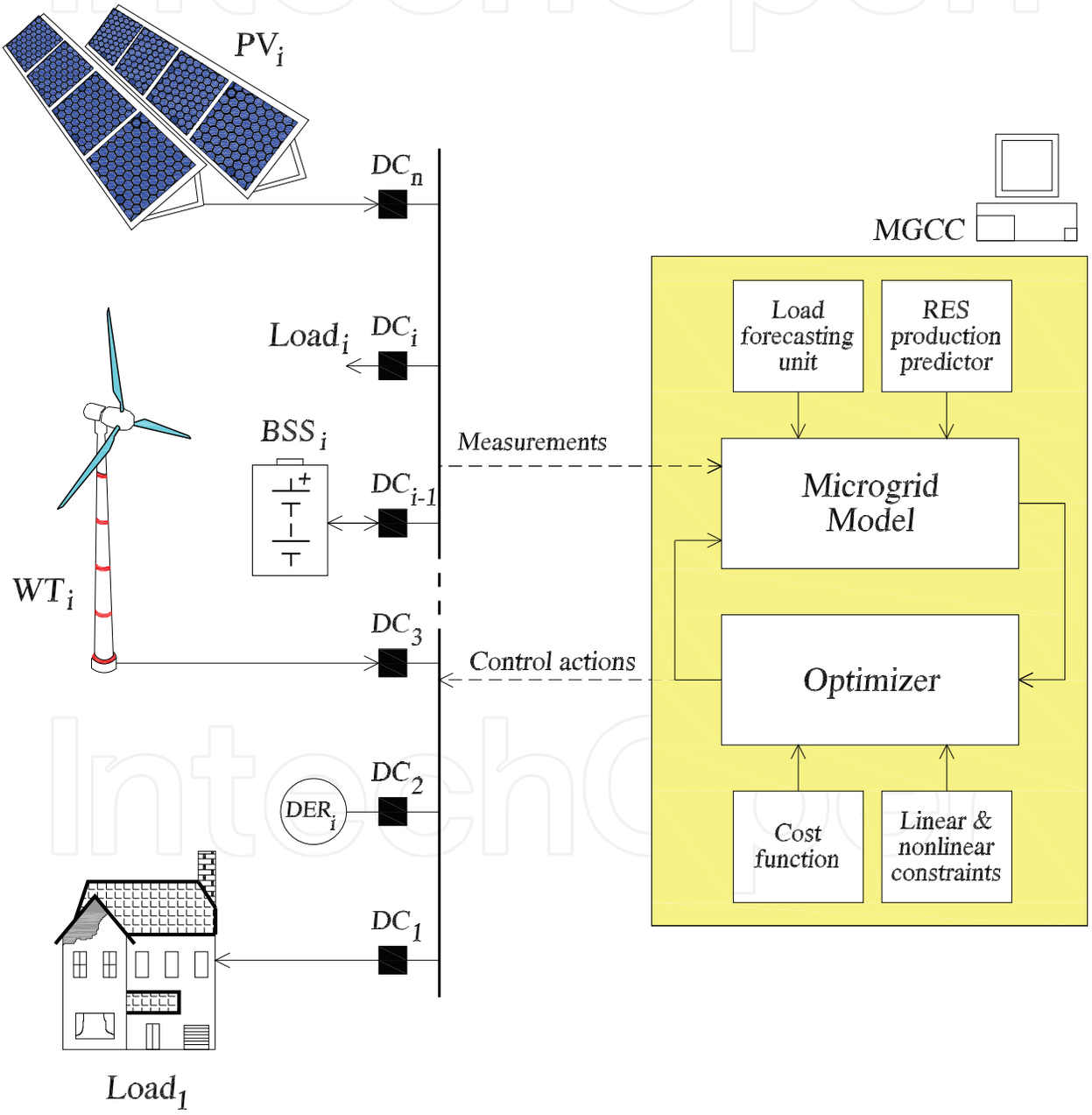

Figure 10. NMPC architecture for a centralized load shedding strategy.

1. Consider the load measurements as constants during the entire prediction horizon N;
2. Use a load predictor based on an artificial neural network (ANN). For this purpose, 20 load profiles from different days of the week for every variable loads in the microgrid were used as training set for configuring a three-layer ANN.

Another approach for predicting the P_{DE} was developed with an autoregressive model with external input (ARX) through a data-based modeling using an adaptive neuro-fuzzy inference system (ANFIS). As in the case of the ANN training algorithm, 20 different generation profiles of the DEG for different days of the week were used as training set for the ANFIS. The ARX configuration developed is the one detailed in Ref. [24]. This modeling procedure does not imply an NR calculation, therefore reducing the computing time of the control algorithm.

Since the voltage magnitude of the microgrid is to be kept within a ±5% range of variation, a static voltage stability index, presented in Ref. [22], is used for defining a secure range of operation of the

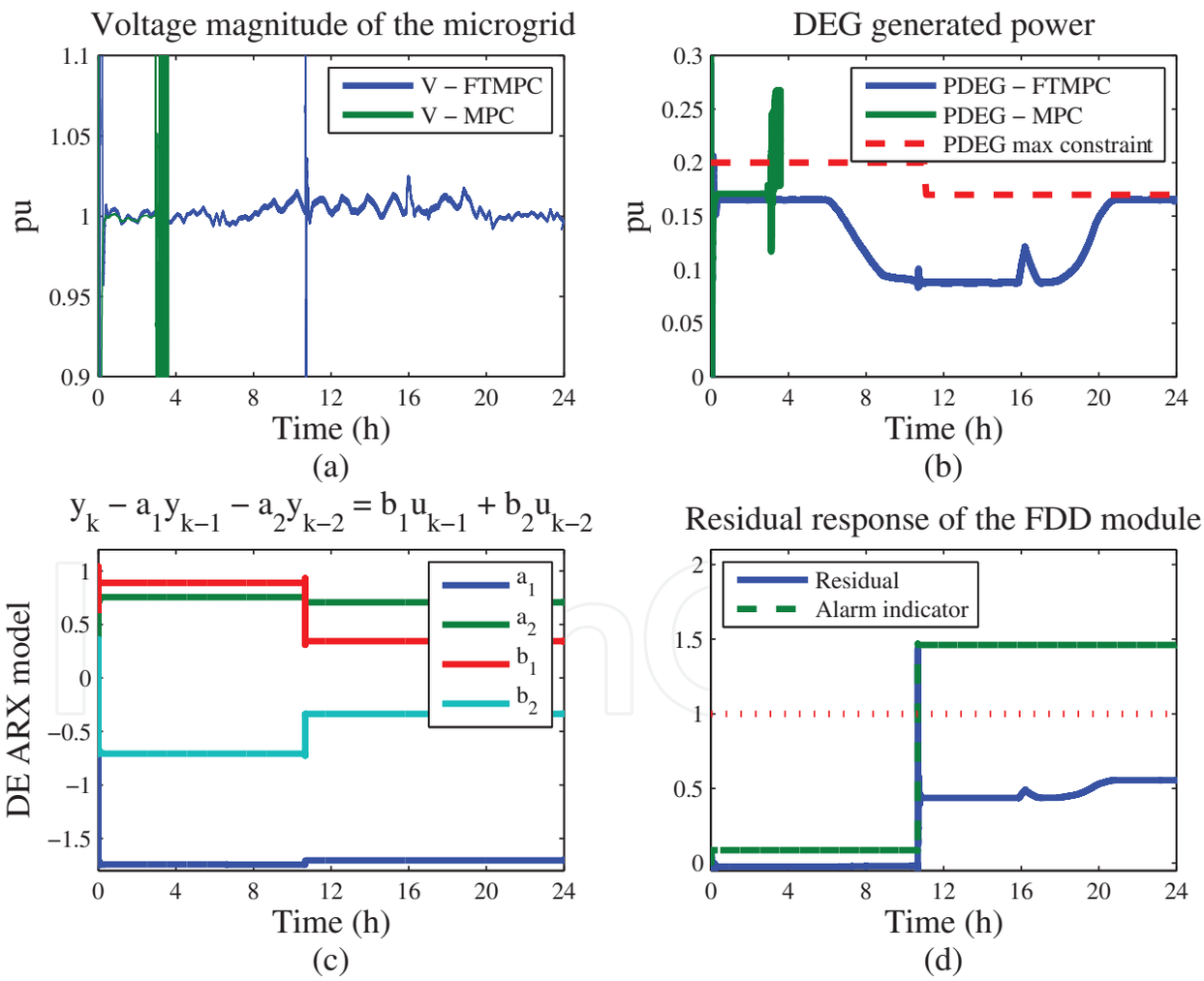

Figure 11. Simulation results of the EMS combining an NMPC algorithm running at the MGCC, and an FTMPC installed at the DEG. (a) Voltage magnitude response comparison between the FTMPC and the MPC systems. (b) Power output of the DEG comparison. (c) ARX model parameters adaptation of the DEG. (d) Residue calculated by the FDD module.

DEG. Consider average generation values of DERs: $P_{WT} = 0.15$, $\Sigma P_{P\ V1,2,3,4} = 0.049$ and $P_{BSS1,2} = 0.035$ in discharge mode and $P_{BSS1,2} = -0.02$ in charge mode, and that the voltage magnitude limits are $0.95 \leq |V| \leq 1.05$, an optimization procedure in which a sweep of the values of P_L, Q_L, and $|V|$ within allowable ranges is performed in order to obtain a secure margin of operation of the microgrid. The secure range of operation for the DE, estimated by the optimization process, is

$$P_{DE} \leq P_{DE}^{+} = 0.2 \tag{14}$$

The control vector **u** calculated by the NMPC algorithm is restricted to be binary. Optimization problems of this type are called mixed-integer nonlinear programming (MINLP) problems. The MINLP package of TOMLAB for MATLAB was used for solving this optimal control problem.

Figure 11 shows the transient response of the voltage magnitude of node-1 of the microgrid in islanded operation. Near 04h00 AM, the DE presents a loss of effectiveness in the servo-mechanism used for fuel injection. Based on the detection of the fault and estimation of the post-fault model of the DE by using a combination of the parity space and Kalman filter methods, a fault-tolerant model-predictive control (FTMPC) has been implemented (see Ref.

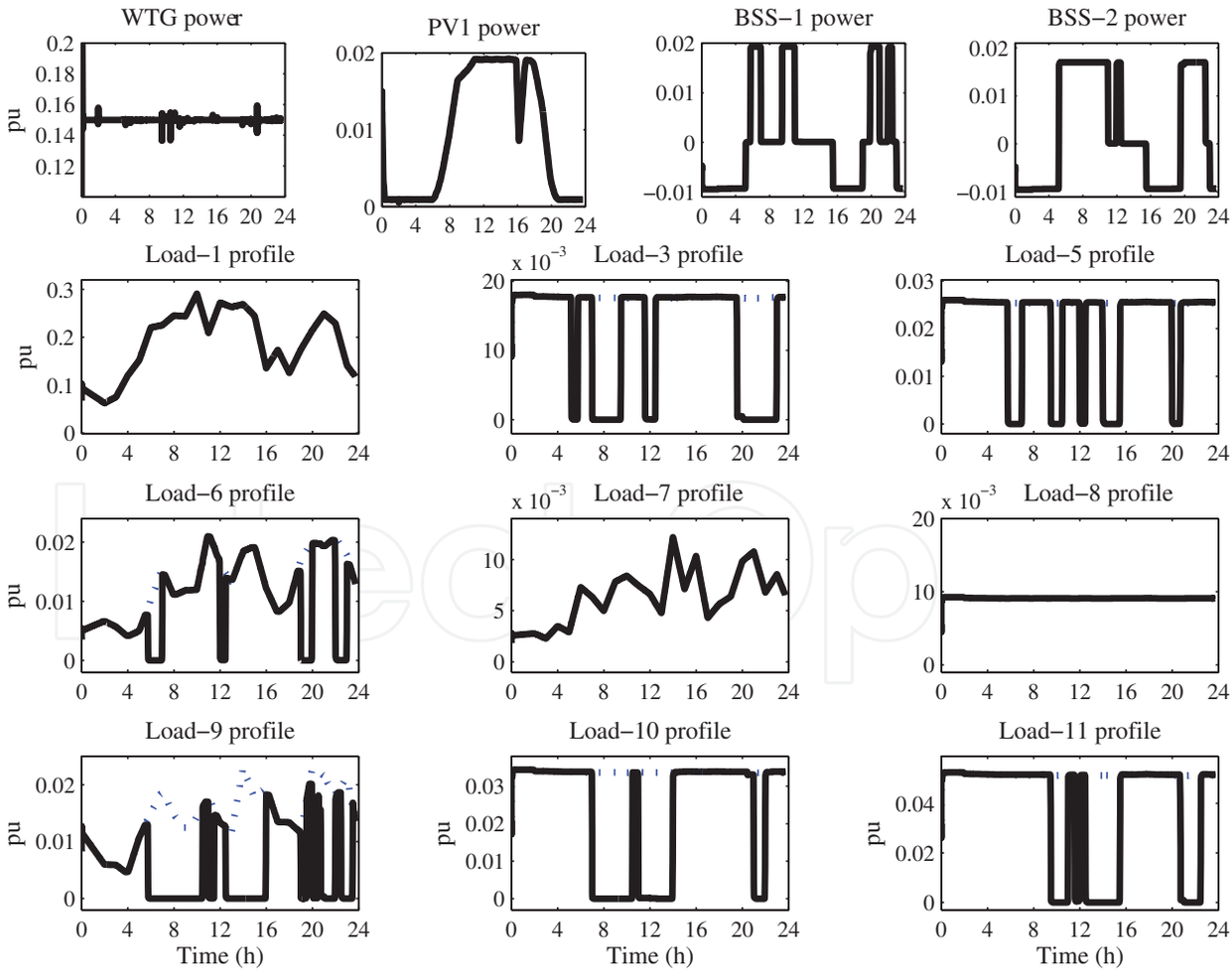

Figure 12. Profiles of RES generated power and load power consumption.

[25] for further details). A simple MPC has also been tested, which causes microgrid instability due to its lack of adaptability to faulty situations.

Figure 12 provides additional information on the NMPC performance by showing the voltage and frequency of the microgrid, and the loads and batteries switching due to the NMPC calculation. Voltage magnitude maintains within the ±5% band (in the weaker bus/node 1) when the microgrid operates in islanded mode. In this operation mode, when no control action is performed, the voltage magnitude constraint is violated. On the other hand, constraints included in the NMPC algorithm are not violated. From **Figure 12**, it is seen that high priority loads L_1, L_7, and L_8 were not disconnected, and at least one load of the low priority loads group kept connected, as it was programmed in the NMPC algorithm. Batteries charge at off-peak times, when there is availability of power from the generation units ($P_{gen} > P_{load}$). Batteries deliver power to the grid when there is a power deficit due to peak consumption. The inclusion of load shedding and battery management in the NMPC algorithm improves the microgrid's overall performance by guaranteeing a reliable and secure operation.

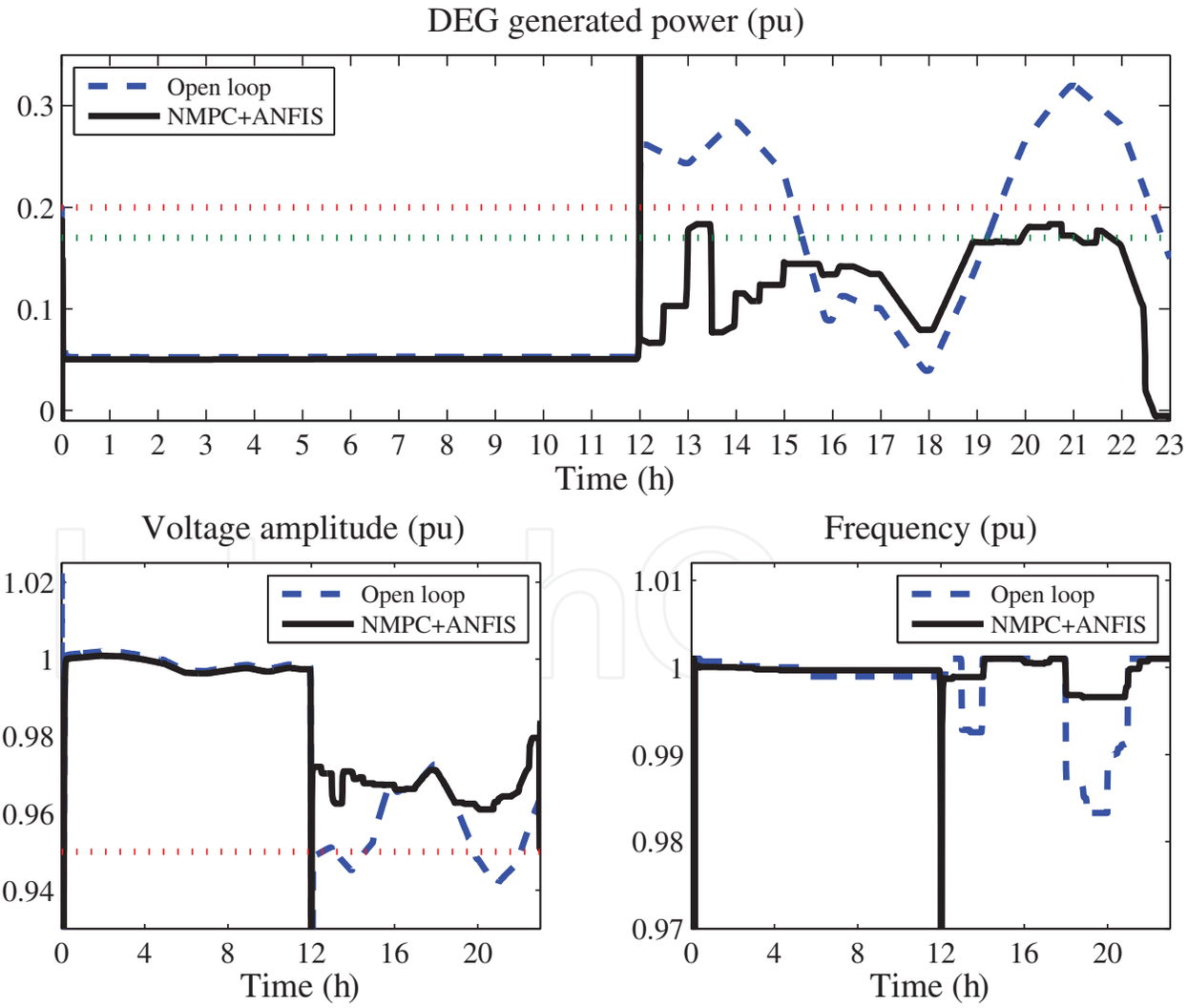

Figure 13. (Upper) P_{DE} when the load shedding NMPC strategy is used (islanding event at 12h00). (Lower left) Voltage magnitude variation; (lower *right) frequency variation.*

In addition to the previous results, **Figure 13** shows the operation of the microgrid under similar conditions of **Figures 11** and **12**. The islanding event occurs at 12h00, and as expected the voltage magnitude variation does not overpass the ±5% variation when the EMS takes decisions on the batteries energy management, and low priority loads to be shed. A similar situation is observed with the frequency deviation from 1 pu, which remains in an acceptable range of variation of maximum 0.05%. By contrast, the simulation of the microgrid operating without the EMS shows an unsecure behavior of the system, violating the $|\Delta V| < \pm 5\%$ operation constraint, and also presenting a much larger frequency variation, as also shown in **Figure 13**.

5. Conclusions

A predictive control scheme that prevents from unbalances between the load demand and the capacity of generation installed in an islanded microgrid is analyzed in this chapter. The NMPC calculates, within an optimization framework, load shedding when necessary as well as the energy management from the batteries in the microgrid. Therefore, an optimal control problem is established, where all the operating conditions of the microgrid are integrated, that is, load priorities for disconnection and batteries charging and discharging cycles. A comparison of some simulation results of the microgrid working with and without the MGCC shows improvements in the reliability of the microgrid when it operates in islanded mode, since simulation results showed the capability of the control strategy of maintaining within safe limits voltage and frequency of the microgrid, as well as a correct balance of generated power and load demand.

Author details

Luis I. Minchala[1,2]*, Youmin Zhang[3] and Oliver Probst[1]

*Address all correspondence to: ismael.minchala@ucuenca.edu.ec

1 Instituto Tecnológico y de Estudios Superiores de Monterrey, Monterrey, NL, México

2 Universidad de Cuenca, Cuenca, AZ, Ecuador

3 Concordia University, Montreal, QC, Canada

References

[1] Constable G, Somerville B. A Century of Innovation—Twenty Engineering Achievements that Transformed Our Lives. Washington, DC: Joseph Henry Press; 2003

[2] Mahmoud MS, Azher Hussain S, Abido MA. Modeling and control of microgrid: An overview. Journal of The Franklin Institute. 2014;**351**(5):2822–2859

[3] Mamo X, Mallet S, Coste T, Grenard S. Distribution automation: The cornerstone for smart grid development strategy. 2009 IEEE Power & Energy Society General Meeting, Calgary, AB, 2009, pp. 1–6

[4] Ha B, Lee S, Shin C, Kwon S, Park S, Park M. Development of intelligent distribution automation system, 2009 Transmission & Distribution Conference & Exposition: Asia and Pacific, Seoul, 2009, pp. 1–4

[5] Craig D, Befus C. Implementation of a Distributed Control System for Electric Distribution Circuit Reconfiguration, 2005/2006 IEEE/PES Transmission and Distribution Conference and Exhibition, Dallas, TX, 2006, pp. 342–347

[6] Hossain E, Kabalci E, Bayindir R, Perez R. Microgrid testbeds around the world: State of art. Energy Conversion and Management. 2014;**86**:132–153

[7] Haritza C, Octavian C, Aitor E, Alvaro L, Amélie HP. Research experimental platforms to study microgrids issues. International Journal on Interactive Design and Manufacturing. 2016;**10**(1):59–71

[8] Masoum M, Dehbonei H, Fuchs E. Theoretical and experimental analyses of photovoltaic systems with voltage and current-based maximum power-point tracking. IEEE Transactions on Energy Conversion. 2002;**17**(12):514–522

[9] Paire D, Miraoui A. Power management strategies for microgrid—A short review, 2013 IEEE Industry Applications Society Annual Meeting, Lake Buena Vista, FL, 2013, pp. 1–9

[10] Minchala-Avila LI, Armijos J, Pesántez D, Zhang Y. Design and implementation of a smart meter with demand response capabilities. Energy Procedia. 2016;**103:**195–200

[11] Chen X, Wei T, Hu S. Uncertainty-aware household appliance scheduling considering dynamic electricity pricing in smart home. IEEE Transactions on Smart Grid. 2013;**4**:932–941

[12] He Y, Jenkins N, Wu J. Smart metering for outage management of electric power distribution networks. Energy Procedia. 2016;**103**:159–164

[13] Blanke M. Diagnosis and Fault-Tolerant Control. Berlin, Heidelberg: Springer-Verlag GmbH; 2003

[14] Zhang Y, Jiang J. Bibliographical review on reconfigurable fault-tolerant control systems. Annual Reviews in Control. 2008;**32**(2):229–252

[15] Grainger JJ, Stevenson WD. Power System Analysis. New York, NY: McGraw-Hill; 1994

[16] Munoz-Aguilar RS, Doria-Cerezo A, Fossas E, Cardoner R. Sliding Mode Control of a Stand-Alone Wound Rotor Synchronous Generator, in IEEE Transactions on Industrial Electronics, 2011;**58**(10):4888–4897

[17] Fuchs EF, Masoum MA. Power Conversion of Renewable Energy Systems. Boulder: Springer; 2011.

[18] Chiasson J, Vairamohan B. Estimating the state of charge of a battery. IEEE Transactions on Control Systems Technology. 2005;**13**(3):465–470

[19] Farrell J, Barth M. Battery state-of-charge estimation. Proceedings of the American Control Conference. 2001;**2**:1644–1649

[20] IEEE Guide for Design, Operation, and Integration of Distributed Resource Island Systems with Electric Power Systems, in IEEE Std 1547.4-2011, vol., no., pp. 1–54, July 20 2011

[21] Rudion K, Orths A, Styczynski ZA, Strunz K. Design of benchmark of medium voltage distribution network for investigation of DG integration, 2006 IEEE Power Engineering Society General Meeting, Montreal, Que, 2006, p. 6

[22] Chen H, Chen J, Shi D, Duan X. Power flow study and voltage stability analysis for distribution systems with distributed generation. In: 2006 IEEE Power Engineering Society General Meeting; 2006. p. 8

[23] Minchala-Avila LI, Garza-Castanon L, Zhang Y, Ferrer HJA. Optimal energy management for stable operation of an islanded microgrid. IEEE Transactions on Industrial Informatics. 2016;**12**(4):1361–1370

[24] Nourzadeh H, Fatehi A, Labibi B, Araabi BN. An experimental nonlinear system identification based on local linear neuro-fuzzy models, 2006 IEEE International Conference on Industrial Technology, Mumbai, 2006, pp. 2274–2279

[25] Minchala-Avila LI, Vargas-Martínez A, Zhang Y, Garza-Castañón LE. A model predictive control approach for integrating a master generation unit in a microgrid, 2013 Conference on Control and Fault-Tolerant Systems (SysTol), Nice, 2013, pp. 674–679

IntechOpen